Chinese Chemical Letters 35 (2024) 108797

Contents lists available at ScienceDirect

Chinese Chemical Letters

journal homepage: www.elsevier.com/locate/cclet

Boron nitride nanofibers enhanced composite PEO-based solid-state polymer electrolytes for lithium metal batteries

Qianqian Song[a,b,1], Yunting Zhang[a,1], Jianli Liang[c], Si Liu[a,d], Jian Zhu[a,*], Xingbin Yan[a,*]

[a] School of Materials Science and Engineering, Sun Yat-Sen University, Guangzhou 510275, China
[b] College of Physics and Materials Science, Tianjin Normal University, Tianjin 300387, China
[c] Department of Chemistry & Center of Super-Diamond and Advanced Films (COSDAF), City University of Hong Kong, Hong Kong 999077, China
[d] Guangdong-Hong Kong-Macao Joint Laboratory for Intelligent Micro-Nano Optoelectronic Technology, School of Physics and Optoelectronic Engineering, Foshan University, Foshan 528225, China

ARTICLE INFO

Article history:
Received 25 May 2023
Revised 3 July 2023
Accepted 10 July 2023
Available online 14 July 2023

Keywords:
Solid-state polymer electrolyte
Boron nitride nanofibers
Lithium metal battery
Ionic conductivity
Li dendrite

ABSTRACT

Polyethylene oxide (PEO)-based solid-state polymer electrolytes (SPEs) are limited by their poor cyclic stability and inferior ionic conductivity for applicating in high-safety, long-cycling and high-energy-density lithium metal batteries. Herein, porous boron nitride nanofibers (BNNFs) are filled into PEO-based SPE, which significantly suppresses Li dendrites growth and enhances the electrochemical performance of Li metal battery. BNNFs with high porosity have more active sites to connect with PEO, which can effectively reduce the crystallinity of the PEO matrix and enhance its ionic conductivity. Moreover, owing to the hardness and good stability of BNNFs, BNNFs/PEO/LiTFSI electrolyte exhibits a wider electrochemical window, better mechanical property and higher thermal stability compared with PEO/LiTFSI electrolyte. Consequently, the Li symmetric cell composed of 1% BNNFs/PEO/LiTFSI performs good cyclic stability (>1800 h), and the Li||1% BNNFs/PEO/LiTFSI||LFP full battery shows obviously improved performances in charge-discharge polarization voltage, discharge specific capacity, rate performance and cyclic stability than the Li||PEO/LiTFSI||LFP battery.

Recent decades have witnessed the rise and prosperity of electric vehicles and numerous electronic devices. As a promising approach for electricity storage, rechargeable Li metal batteries are earning increased attention due to the high theoretical specific capacity (3860 mAh/g) and the lowest electrochemical potential (−3.04 V versus standard hydrogen electrode) of the metallic lithium anode [1,2]. However, the practical application of Li metal batteries is hindered by several fatal safety issues: short circuits of battery and fire of flammable electrolyte which are caused by the growth of Li dendrites [3–5]. Applying solid-state electrolytes (SSEs) to replace the conventional flammable liquid electrolyte is a promising strategy to solve this problem, which can not only physically hinder the dendrites growth of Li metal anode but also prevent the side effects of electrolyte and electrode [6,7].

Ideal SSEs must be non-flammable and mechanically rigid while exhibiting comparable or even superior ionic conductivity compared to liquid electrolytes. Inorganic SSEs have excellent mechanically rigid and relatively high ionic conductivity (10^{-3}–10^{-4} S/cm) but suffer from insufficient compatibility with the electrode [8–12]. On the contrary, permeable and processible organic polymer SSEs show remarkable interfacial stability, making them promising materials for replacing liquid electrolytes [13,14]. With high dielectric constant and favorable Li ions solvation, while having low cost and lightweight, polyethylene oxide (PEO) was demonstrated as an outstanding polymer matrix [15–17]. However, the poor mechanical strength and thermal stability of the PEO-based SPEs severely restricted their effectiveness of suppressing the growth of Li dendrite. In addition, the insufficiency of ionic conductivity, low lithium ions transference number (t_{Li^+}), and narrow electrochemical window are other problems yet to be addressed [18–20]. Adding Li ion conductors such as $Li_7La_3Zr_2O_{12}$ (LLZO), $Li_{3x}La_{2/3-x}TiO_3$ (LLTO), and $Li_{1.5}Al_{0.5}Ge_{1.5}(PO_4)_3$ (LAGP) into the SPEs system to introduce additional transference of Li ion is an efficient method to improve the electrochemical performance [21–24]. However, this method significantly increases the cost of the battery and impedes the large-scale application of PEO-based SPEs. Blending inorganic additives which are passive for Li^+ conduction, such as SiO_2, TiO_2, and Al_2O_3 has been proven another effective improving strategy. These passive inorganic fillers

* Corresponding authors.
E-mail addresses: zhuj88@mail.sysu.edu.cn (J. Zhu), yanxb3@mail.sysu.edu.cn (X. Yan).
[1] These authors contributed equally to this work.

https://doi.org/10.1016/j.cclet.2023.108797
1001-8417/

as reinforcements can provide interfaces to promote the ionic transfer and also improve the physical and mechanical properties of PEO-based SPEs [25–27]. However, as of today, the performance of these passive inorganic fillers still cannot meet the demands for practical application. So it is still urgent to explore new passive inorganic fillers with better performance and higher cost efficiency.

Hexagonal boron nitride (h-BN) materials with graphene-like structure and marvelous mechanical strength [28] show great potential as passive inorganic fillers for SPEs. h-BN materials are electrical insulator inherently, due to the partially ionic properties and unique orbital properties of their B-N bonds, and have excellent thermal and electrochemical stability [29,30]. Notably, the Lewis acid feature of B atoms in boron nitride (BN) plays the role of an anchor point to draw anions and promote the interaction of Lewis acid and Lewis base, thereby inducing the dissociation and uniform distribution of Li^+ and improving the electrochemical performance of additive-filled SPEs. However, although there are a few studies demonstrating that adding BN leads to the increase of ionic conductivity and the strength of electrolyte, which contributes to the improvement of battery efficiency [31–33], effects of BN on inhibiting the growth of Li dendrites and enhancing the cyclic stability of Li metal batteries are not satisfactory. Therefore, it is necessary to develop novel boron nitride fillers with better Li dendrites inhibition properties to make up for the deficiency.

In this work, porous boron nitride nanofibers (BNNFs) as novel filler were added into PEO/LiTFSI to enhance the properties of PEO-based SPEs. The BNNFs/PEO/LiTFSI with the optimized amount of filled BNNFs (1 wt%) shows the best performance with high ionic conductivity, wide electrochemical window, large Li-ion transference number, efficient Li dendrite suppression and excellent cyclic stability of Li symmetric cell (>1800 h). Owing to their microporous/mesoporous structure and higher specific surface area of BNNFs, they can be linked with PEO more closely to effectively reduce the crystallinity of PEO as well as improve the mechanical properties and thermal stability of the PEO matrix. In addition, Li||1% BNNFs/PEO/LiTFSI||LFP full battery shows lower charge-discharge polarization voltage, higher discharge specific capacity, better rate performance and cyclic stability. Therefore, BNNFs have been demonstrated as an ideal filler for the modification of PEO-based SPEs to improve Li metal batteries performance.

BNNFs were characterized in detail to reveal their physicochemical properties. The obvious B-N stretching vibration (~1370 cm^{-1}) and B-N-B bending vibration (~790 cm^{-1}) in FT-IR spectrum (Fig. S1 in Supporting information) prove the successful synthesis of h-BN [30,34]. In addition, the -OH and -NH_2 stretching vibration peaks at ~3000 cm^{-1} to ~4000 cm^{-1} indicate numerous active groups on the surface of BNNFs [35], which can facilitate their combination with the PEO matrix. In the XRD pattern (Fig. S2 in Supporting information), the large broadening diffraction peaks corresponding to the (002), (100), and (101) planes of h-BN infer the small crystal grains and relatively low crystallinity of BNNFs [36]. The SEM image in Fig. S3 (Supporting information) presents a uniformly fibrous morphology of the prepared BNNFs with a large aspect ratio. TEM image (Fig. S4 in Supporting information) further confirmed the fibrous morphology of BNNFs with a diameter of about 300 nm. A considerable number of bright spots on fibers can be attributed to the pore structure of BNNFs. The inset high-resolution TEM image, combined with the XRD pattern, further verifies the low crystallinity of BNNFs. Lots of CO, NH_3, N_2 and H_2O gaseous molecules were generated in the pyrolysis process of M·B_2 precursor. These small molecules would escape from the precursor matrix, resulting in a rich porous structure and a large specific surface area of as-prepared BNNFs [37]. In order to acquire precise properties on the pore structure of BNNFs, an N_2 adsorption-desorption test was carried out and the result is shown in Fig. S5 (Supporting information). An I-type isotherm with an H4-type hysteresis loop demonstrates the existence of high-density nanopores in the sample [38]. The specific surface area calculated by the BET method is 1036 m^2/g, illustrating an eminently large specific surface area of BNNFs. The pore size distribution is mainly micropores below 2 nm and mesoporous pores around 4 nm, calculated by the DFT method shown in Fig. S6 (Supporting information). The porosity of BNNFs may significantly affect the electrochemical performance of the BNNFs-filled PEO-based SPEs.

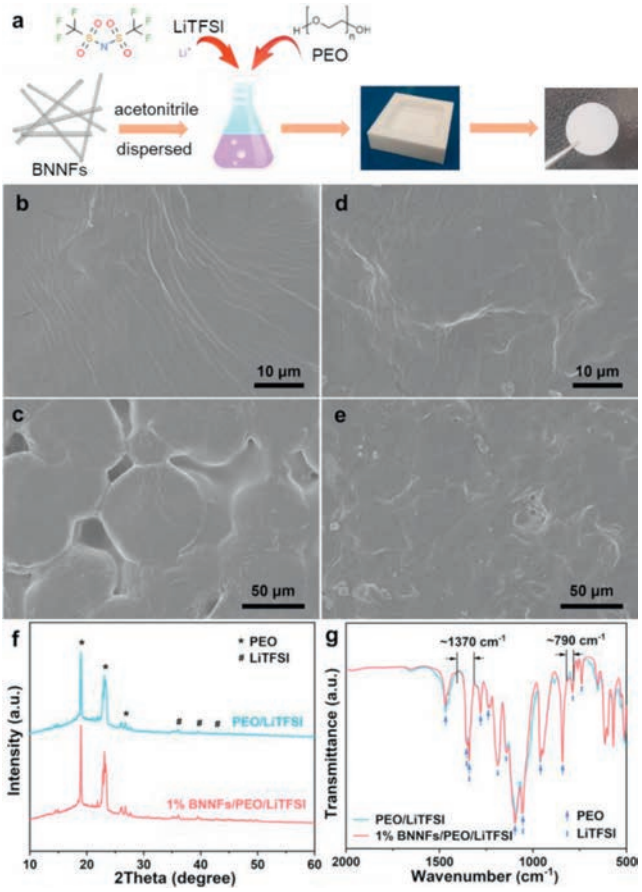

Fig. 1. (a) Schematic diagram of the preparation process of PEO-based SPEs, SEM images of (b, c) PEO/LiTFSI and (d, e) 1% BNNFs/PEO/LiTFSI, (f) XRD patterns and (g) FT-IR spectra of PEO/LiTFSI and 1% BNNFs/PEO/LiTFSI.

The PEO-based SPEs were prepared by the solvent casting method and the schematic diagram of the preparation process is shown in Fig. 1a. The thickness of the obtained PEO-based SPEs is about 160 μm. Wrinkles on the surface of PEO/LiTFSI (Fig. 1b) and 1% BNNFs/PEO/LiTFSI (Fig. 1d) are observed on high-magnification SEM images, due to the intrinsic properties of PEO [33]. Observed at lower magnification, the PEO/LiTFSI is composed of multiple grains with a diameter of about 50 μm that are connected relevantly (Fig. 1c). There are grooves and grain boundaries between the grains, indicating that the crystallinity of PEO/LiTFSI is relatively high. On the contrary, 1% BNNFs/PEO/LiTFSI do not include obvious grain structure, and the surface was relatively smooth and uniform (Fig. 1e), indicating that adding BNNFs optimized the structure of the PEO-based SPEs. The XRD patterns of PEO/LiTFSI and 1% BNNFs/PEO/LiTFSI (Fig. 1f) are very similar, mainly PEO and LiTFSI diffraction peaks [39,40]. The introduced 1% BNNFs show no apparent diffraction peak and no noticeable effect on the XRD pattern of PEO/LiTFSI, mainly due to the small amount and the low crystallinity of BNNFs. The FT-IR spectra of PEO/LiTFSI and 1% BNNFs/PEO/LiTFSI in Fig. 1g show almost overlapped profiles with absorption peaks mainly attributed to the vibration of PEO and LiTFSI

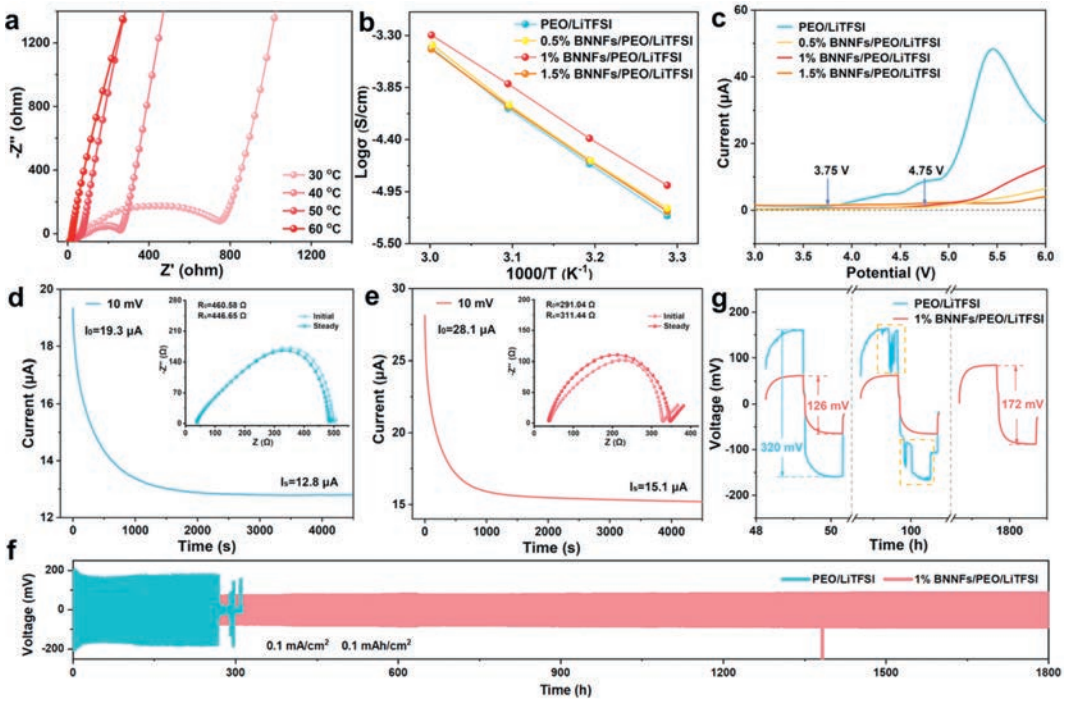

Fig. 2. (a) EIS plots of 1% BNNFs/PEO/LiTFSI at different temperatures. (b) Ionic conductivity versus temperature, and (c) LSV of PEO-based SPEs with different BNNFs additions. (d, e) Chronoamperometry curves of PEO/LiTFSI and 1% BNNFs/PEO/LiTFSI, the inset is the EIS plots before and after the test. (f) Galvanostatic deposition/stripping voltage profiles of Li||Li symmetric cells assembled by PEO/LiTFSI and 1% BNNFs/PEO/LiTFSI at 0.1 mA/cm^2 and (g) amplified voltage profiles at 50, 100, and 1800 h.

[41]. The B-N vibration peaks at ~1370 cm^{-1} and ~790 cm^{-1} are slightly stronger in 1% BNNFs/PEO/LiTFSI than those in PEO/LiTFSI, due to the addition of 1% BNNFs.

Fig. 2a is the Nyquist plots of 1% BNNFs/PEO/LiTFSI at different temperatures. The intrinsic resistance at 30–60 °C was deduced to be 757.60, 259.27, 68.75, and 21.02 Ω, respectively. The ionic conductivity of PEO-based SPEs was calculated from the electrical resistance, the thickness of SPEs, and the effective contact area between the electrolyte and the electrode. In order to explore the optimal addition amount of BNNFs, PEO-based SPEs with 0.5%, 1%, and 1.5% BNNFs were prepared, respectively, and their ionic conductivities were tested. As shown in Fig. 2b, the ionic conductivity of PEO/LiTFSI at 30 °C is 6.24 × 10^{-6} S/cm. The ionic conductivity gradually increases with increasing temperature and reaches 3.75 × 10^{-4} S/cm at 60 °C. The ionic conductivity at 30–60 °C was only slightly higher when 0.5% BNNFs were added into PEO/LiTFSI, but was significantly improved with 1% BNNFs added. It reaches 1.31 × 10^{-5} S/cm at 30 °C and 5.05 × 10^{-4} S/cm at 60 °C. The more obvious increase of ionic conductivity at room temperature may be attributed to the porosity and higher specific surface area of BNNFs, which facilitate its cross-link with PEO to effectively reduce the crystallinity of the PEO matrix. However, the ionic conductivity of BNNFs/PEO/LiTFSI decreased when the addition amount of BNNFs was further increased to 1.5%, indicating that 1% BNNFs was the optimized addition amount in this system. When the addition amount was too small, it had negligible effect on the PEO matrix and its ionic conductivity. On the contrary, when the additive amount increases to 1.5%, the agglomeration and sedimentation of BNNFs may occur and have negative impacts on the ionic conductivity [16]. According to the classical Arrhenius equation $\sigma(T) = A\exp(-E_a/RT)$, the activation energy E_a of PEO-based SPEs can be calculated from the relationship between the ionic conductivity σ and the corresponding temperature in Fig. 2b, where T is the absolute temperature, A is the pre-exponential factor and R is the molar gas constant [41–43]. When 1% BNNFs were added, the E_a of PEO-based SPEs was 0.49 eV, which was smaller than that without BNNFs (0.54 eV). The lower the E_a, the faster ions migrate. Therefore, the ion mobility of 1% BNNFs/PEO/LiTFSI is higher than that of PEO/LiTFSI. In addition, Figs. 2d and e show the chronoamperometry curves of PEO/LiTFSI and 1% BNNFs/PEO/LiTFSI, respectively; the insets are the EIS plots before and after the test. The calculated Li ion transference number (t_{Li^+}) of PEO/LiTFSI is 0.17, and for 1% BNNFs/PEO/LiTFSI is 0.18. It was found that the interaction between the BNNFs surface and PEO can promote the local relaxation and chain segment motion of Li^+. On the other hand, BNNFs may also interact with LiTFSI, making LiTFSI more prone to dissociation, increasing the proportion of free Li^+, and improving Li^+ mobility [31].

Fig. 2c shows the LSV of PEO-based SPEs with various amounts of BNNFs additions. PEO/LiTFSI will undergo oxidative degradation when the voltage is greater than 3.75 V [44], while the current of PEO-based SPEs with different addition amounts of BNNFs did not climb until the voltage was higher than 4.75 V, indicating a significant expansion of the electrochemical stability window. Due to the excellent electrochemical stability, BNNFs can effectively reduce the degree of anion oxidation at high potential, therefore PEO-based SPEs with BNNFs addition can meet the requirements of most high-voltage Li batteries.

Evaluating the stability of Li||Li symmetric cells composed of SPEs during galvanostatic charge-discharge (GCD) is of great significance to examining the long cycle life of the batteries. During the repeated deposition/stripping of Li on the surface of the Li metal, the uneven deposition/stripping of metallic Li will induce the growth of Li dendrites, which will pierce the SPEs membrane eventually and short-circuit the battery. Fig. 2f shows the galvanostatic deposition/stripping voltage profiles of PEO/LiTFSI and 1% BNNFs/PEO/LiTFSI composed Li||Li symmetric cells at a current density of 0.1 mA/cm^2 and a specific capacity of 0.1 mAh/cm^2. The PEO/LiTFSI symmetric cell experienced an obvious short circuit after about 270 h, while the 1% BNNFs/PEO/LiTFSI symmetric cell cycled stably for more than 1800 h. The ionic conductivity and symmetric cell cyclic stability of 1% BNNFs/PEO/LiTFSI compared

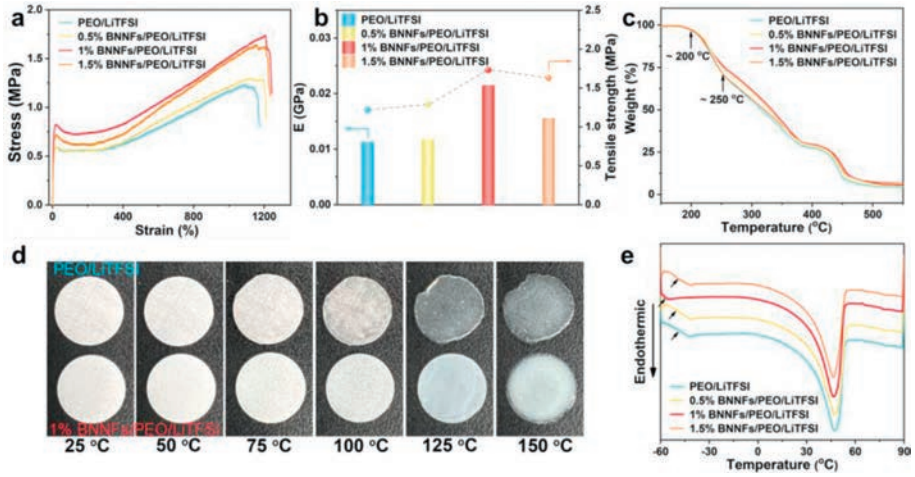

Fig. 3. (a) Stress–strain curves, (b) Young's modulus and tensile strength, (c) TG curves of PEO-based SPEs with different amounts of BNNFs additions. (d) Photos of heating experiment of PEO/LiTFSI and 1% BNNFs/PEO/LiTFSI in the air at 25–150 °C and (e) DSC curves of PEO-based SPEs with different amounts of BNNFs additions.

to those of other inorganic filler enhanced PEO-based SPEs are shown in Table S1 (Supporting information). The amplified voltage profiles (Fig. 2g) show a much smaller overpotential of the 1% BNNFs/PEO/LiTFSI symmetric cell of 126 mV than that of the PEO/LiTFSI symmetric cell of 320 mV, after cycling for 50 h. Low polarization implies a small energy barrier for Li-ion nucleation, which is conducive to relatively uniform deposition [45]. In detail, the amplified voltage profile of the PEO/LiTFSI symmetrical cell fluctuates irregularly after cycling for 100 h, which can be generally attributed to the Li dendrites caused micro-short circuit. This phenomenon indicates that the PEO/LiTFSI symmetric cell become instable since 100 h, and totally disabled at 270 h. As comparison, the amplified voltage profile of 1% BNNFs/PEO/LiTFSI symmetric cell still shows a stable and low overpotential (172 mV) even after 1800 h, demonstrating excellent effects of the addition of 1% BNNFs on strengthening PEO-based SPEs and inhibiting the growth of Li dendrites.

In order to further verify the inhibition of PEO-based SPEs with BNNFs addition on the growth of Li dendrite, postmortem analysis of symmetric cells after 50 cycles was carried out. The surface morphology of Li metal was observed by SEM (Fig. S7 in Supporting information). Compared with the original smooth Li metal surface prior the cycle, a large number of cracks and protrusions appeared on the Li electrode surface of the PEO/LiTFSI assembled Li symmetric cell after 50 cycles (Fig. S7a). In contrast, the Li electrode surface of Li symmetric cell assembled with 1% BNNFs/PEO/LiTFSI has less roughness (Fig. S7b). So it was confirmed that the addition of 1% BNNFs in PEO-based SPEs was beneficial to prevent the growth of Li dendrites.

The mechanical properties of SPEs in Li metal batteries are very important since only the SPEs membrane with sufficient strength (high Young's modulus) can inhibit the growth of Li dendrites during the repeated deposition/stripping of Li metal on the electrode surface. Here, the strain–stress curves of PEO-based SPEs were obtained by uniaxial tensile test, and Young's modulus and tensile strength were calculated. As shown in Figs. 3a and b, the elongation at break, Young's modulus, and tensile strength of the samples all increased first and then decreased as the addition of BNNFs increased from 0% to 1.5%. 1% BNNFs/PEO/LiTFSI exhibited the best mechanical properties among all samples, which is consistent with the changing trend of ionic conductivity. Compared with PEO/LiTFSI, Young's modulus (0.02 GPa) of 1% BNNFs/PEO/LiTFSI is twice that of PEO/LiTFSI (0.01 GPa), and its tensile strength is also 0.51 MPa higher than that of PEO/LiTFSI. Since Young's modulus is a direct reflection of hardness and tensile strength, represents the amount of stress the samples can bear before breaking, PEO-based SPEs with BNNFs addition with better mechanical properties can effectively inhibit the growth of Li dendrites and the puncture of the electrolyte membrane [46,47]. It is well accepted that adding inorganic filler helps PEO intertwine and cross-link with its surface. Due to their microporous/mesoporous structure and high specific surface area, BNNFs provide more physical cross-linking centers than other inorganic filler, which makes the cross-linking more intense, and mechanical properties of PEO-based SPEs with BNNFs addition better.

In addition to mechanical properties, thermal stability is also crucial for the safety of SPEs in Li-metal batteries. Fig. 3c shows the TG curves of PEO-based SPEs with different amounts of BNNFs additions in air, all samples with BNNFs additive acquire enhanced thermal stability compared with PEO/LiTFSI, and 1% BNNFs/PEO/LiTFSI exhibits superior performance among them. Obvious weight loss of the PEO-based SPEs can be observed when the temperature exceeds 200 °C, until 500 °C. Compared to the PEO/LiTFSI without BNNFs whose mass decreases rapidly with the increase in temperature, the addition of BNNFs can significantly enhance the thermal stability of PEO-based SPEs and delay the temperature at which weight loss occurs, especially the decomposition of PEO at about 250 °C [48]. The magnified TG curves between 150 °C and 350 °C are shown in Fig. S8 (Supporting information). The photos of the heating experiment of PEO/LiTFSI and 1% BNNFs/PEO/LiTFSI membranes in the air at different temperatures are shown in Fig. 3d. The PEO/LiTFSI membrane experienced a certain volume shrinkage at 75 °C and became partially translucent (a typical sign for the softening and melting of PEO) at 100 °C. As comparison, the color and state of the 1% BNNFs/PEO/LiTFSI membrane did not change until 125 °C, and there was no volume shrinkage in the whole test temperature range. The prominent heat conductivity and thermal stability of BNNFs are conducive to the thermal stability of PEO-based SPEs and Li metal batteries composed of PEO-based SPEs [39].

The crystallinity and internal fragment disorder of a polymer can be assessed from its DSC results. As shown in Fig. 3e, the glass transition temperature (T_g) of PEO-based SPEs decreases significantly from −47.36 °C of PEO/LiTFSI to −56.69 °C of 1% BNNFs/PEO/LiTFSI, and the melting temperature (T_m) also drops slightly from 49.10 °C to 48.28 °C. Although no significant changes are seen in XRD patterns, the more sensitive DSC results illustrate that the addition of 1% BNNFs reduces the crystallinity of

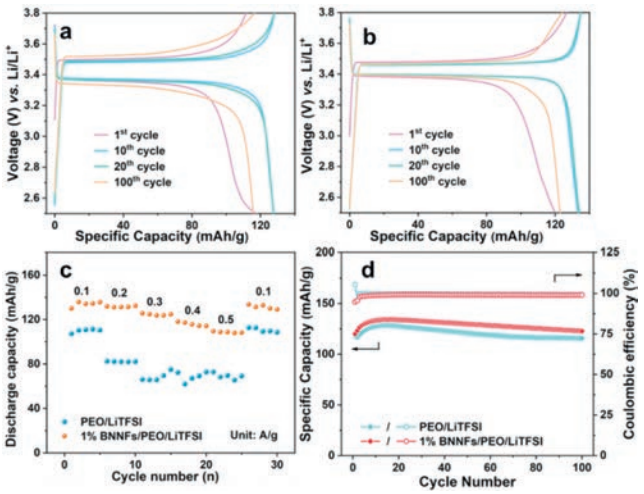

Fig. 4. Charge-discharge curves of (a) Li||PEO/LiTFSI||LFP and (b) Li||1% BNNFs/PEO/LiTFSI||LFP at the 1st, 10th, 20th, and 100th cycles. (c) Rate capacity, and (d) cyclic stability of Li||PEO/LiTFSI||LFP and Li||1% BNNFs/PEO/LiTFSI||LFP at 60 °C and 0.1 A/g.

the PEO/LiTFSI hybrid matrix and promotes its chain activity which makes Li ions movement easier in the electrolyte, thus improving the ionic conductivity of PEO-based SPEs [49].

To evaluate the electrochemical performance of PEO-based SPEs in full batteries, asymmetric Swagelok cells with Li metal anode and $LiFePO_4$ cathode were assembled and tested. Figs. 4a and b show charge and discharge curves of Li||PEO/LiTFSI||LFP and Li||1% BNNFs/PEO/LiTFSI||LFP from 2.5 V to 3.8 V at the 1st, 10th, 20th and 100th cycle, respectively. The charge-discharge reaction curves of the two full batteries are consistent with the typical curve of lithium metal batteries with $LiFePO_4$ cathode [23]. The voltage gap between charge/discharge voltage platforms of Li||1% BNNFs/PEO/LiTFSI||LFP is significantly smaller than that of Li||PEO/LiTFSI||LFP, indicating that the 1% BNNFs/PEO/LiTFSI electrolyte provides a higher Li^+ mobility and a stable interface between electrolyte and electrode [50]. After 10 cycles, the voltage gaps of the two full batteries decrease slightly and remain stable for a period. After 100 cycles, the voltage gap between charge and discharge voltage platform of Li||PEO/LiTFSI||LFP increases significantly while that of Li||1% BNNFs/PEO/LiTFSI||LFP increases slightly compared with that after 10 cycles, indicating no obvious polarization on 1% BNNFs/PEO/LiTFSI electrolyte/electrode interface and its excellent electrochemical stability.

Fig. 4c shows the rate performance of full batteries at different current densities from 0.1 C to 0.5 C. The discharge capacity of Li||1% BNNFs/PEO/LiTFSI||LFP is higher than that of Li||PEO/LiTFSI||LFP at all current densities, especially at higher current density. The excellent rate performance is attributed to not only the higher ionic conductivity of 1% BNNFs/PEO/LiTFSI, but also the stability of the interface between 1% BNNFs/PEO/LiTFSI and the electrode. Furthermore, cyclic stability is another important parameter to evaluate its applicability in practical applications. Therefore, the cyclic stability of two full batteries was further evaluated by GCD at 0.1 A/g. As shown in Fig. 4d, the discharge specific capacities of PEO/LiTFSI and 1% BNNFs/PEO/LiTFSI are 117.53 and 120.05 mAh/g, respectively, in the first cycle. During the first 10 cycles, they gradually increase to 127.74 and 133.36 mAh/g, respectively, corresponding to the activation of LFP. Thereafter, discharge specific capacities of both full batteries remain relatively stable and decreased slightly. After 100 cycles, the discharge specific capacity of PEO/LiTFSI and 1% BNNFs/PEO/LiTFSI batteries remain at 115.77 and 122.83 mAh/g, respectively, and their capacity retention are 90.63% and 92.11% of the highest capacity. The performance of 1% BNNFs/PEO/LiTFSI is better than that of PEO/LiTFSI in terms of discharge specific capacity and cyclic stability. Considering that the two full batteries are composed of the same components except for the BNNFs filler, therefore the different electrochemical properties can be attributed to the enhanced Li^+ transport in the PEO-based SPEs and electrode/electrolyte interface stability by the addition of BNNFs.

In summary, porous BNNFs were added as a filler into PEO-based SPE to enhance the ionic conductivity and suppress Li dendrites. Benefiting from the microporous/mesoporous structure, the porous BNNFs filler can form more crosslinks with the PEO matrix to effectively reduce its crystallinity and enhance its ionic conductivity. Coupled with the excellent hardness and thermal conductivity of BNNFs, the PEO-based SPE filled with porous BNNFs exhibited better mechanical property and higher thermal stability than the original PEO/LiTFSI electrolyte. Therefore, the Li symmetric cell composed of 1% BNNFs/PEO/LiTFSI could cycle stably for more than 1800 h, and the Li||1% BNNFs/PEO/LiTFSI||LFP full battery exhibited a smaller charge–discharge polarization voltage, a higher discharge specific capacity, better rate performance and cyclic stability than the Li||PEO/LiTFSI||LFP full battery. Taking porous BNNFs as filler for PEO-based SPEs may provide an inspirational spark for the development of organic SPEs in Li metal batteries.

Declaration of competing interest

The authors declare no competing financial interest to influence the work reported in this paper.

Acknowledgments

This work was financially supported by the National Key R&D Program of China (No. 2022YFB2402600), National Natural Science Foundation of China (Nos. 22279166, 52203346), Basic and Applied Basic Research Foundation of Guangdong Province (Nos. 2021A1515110168, 2022B1515120019), Basic and Applied Basic Research Foundation of Guangzhou (No. 202201011322), Fundamental Research Funds for the Central Universities, Sun Yat-Sen University (Nos. 22qntd0101 and 22dfx01) and Special Fund of Science and Technology Innovation Cultivation for College Students in Guangdong Province (No. pdjh2021b0022).

Supplementary materials

Supplementary material associated with this article can be found, in the online version, at doi:10.1016/j.cclet.2023.108797.

References

[1] M.J. Lee, J. Han, K. Lee, et al., Nature 601 (2022) 217–222.
[2] Y. Liu, D. Lin, Y. Jin, et al., Sci. Adv. 3 (2017) eaao0713.
[3] J.S. Kim, H. Kim, M. Badding, et al., J. Mater. Chem. A 8 (2020) 16892–16901.
[4] J. Gu, Q. Zhu, Y. Shi, et al., ACS Nano 14 (2020) 891–898.
[5] H. Duan, L. Li, K. Zou, et al., ACS Appl. Mater. Interfaces 13 (2021) 57380–57391.
[6] D.M. Reinoso, M.A. Frechero, Energy Storage Mater. 52 (2022) 430–464.
[7] L. Li, J. Wang, L. Zhang, et al., Energy Storage Mater. 45 (2022) 1062–1073.
[8] X. Han, Y. Gong, K. Fu, Nat. Mater. 16 (2017) 572–579.
[9] H. Zhao, J. Zhong, Y. Qi, et al., Chem. Eng. J. 465 (2023) 143032.
[10] K. Liang, H. Zhao, J. Li, et al., Small 2 (2023) 2207562.
[11] P. Wei, X. Sun, Z. He, et al., Fuel 339 (2023) 127303.
[12] K. Liang, H. Zhao, J. Li, et al., Appl. Surf. Sci. 615 (2023) 156412.
[13] Y. Su, X. Rong, A. Gao, et al., Nat. Commun. 13 (2022) 4181.
[14] M. Ge, X. Zhou, Y. Qin, et al., Chin. Chem. Lett. 33 (2022) 3894–3898.
[15] J. Wan, J. Xie, D.G. Mackanic, et al., Mater. Today Nano 4 (2018) 1–16.
[16] J. Feng, L. Wang, Y. Chen, et al., Nano Converg. 8 (2021) 2.
[17] L. Li, Y. Deng, H. Duan, et al., J. Energy Chem. 65 (2021) 319–328.
[18] W. Tang, S. Tang, X. Guan, et al., Adv. Funct. Mater. 29 (2019) 1900648.
[19] Q. Yu, K. Jiang, C. Yu, et al., Chin. Chem. Lett. 32 (2021) 2659–2678.
[20] Y. Na, Z. Chen, Z. Xu, et al., Chin. Chem. Lett. 33 (2022) 4037–4042.

[21] J. Zheng, M. Tang, Y. Hu, et al., Angew. Chem. 128 (2016) 12726–12730.
[22] W. Liu, S.W. Lee, D. Lin, et al., Nat. Energy 2 (2017) 17035.
[23] X. Wang, H. Zhai, B. Qie, et al., Nano Energy 60 (2019) 205–212.
[24] L. Li, Y. Deng, G. Chen, J. Energy Chem. 50 (2020) 154–177.
[25] J. Weston, B. Steele, Solid State Ion. 7 (1982) 75–79.
[26] D. Lin, W. Liu, Y. Liu, et al., Nano Lett. 16 (2016) 459–465.
[27] J. Adebahr, A.S. Best, N. Byrne, et al., Phys. Chem. Chem. Phys. 5 (2003) 720–725.
[28] C. Zhi, Y. Bando, C. Tang, et al., Adv. Mater. 21 (2009) 2889–2893.
[29] Q. Weng, X. Wang, X. Wang, et al., Chem. Soc. Rev. 45 (2016) 3989–4012.
[30] A. Pakdel, Y. Bando, D. Golberg, Chem. Soc. Rev. 43 (2014) 934–959.
[31] J. Shim, H.J. Kim, B.G. Kim, et al., Energy Environ. Sci. 10 (2017) 1911–1916.
[32] Z. Zhang, R.G. Antonio, K.L. Choy, J. Power Sources 435 (2019) 226736.
[33] Y. Li, L. Zhang, Z. Sun, et al., J. Mater. Chem. A 8 (2020) 9579–9589.
[34] J. Liang, Q. Song, J. Lin, et al., Chem. Eng. J. 373 (2019) 616–623.
[35] Q. Song, J. Liang, Y. Fang, et al., Chem. Eng. J. 394 (2020) 124985.
[36] J. Liang, J. Lin, R. Li, et al., Ceram. Int. 43 (2017) 15402–15409.
[37] J. Li, J. Lin, X. Xu, et al., Nanotechnology 24 (2013) 155603.
[38] R. Evans, P. Tarazona, Phys. Rev. Lett. 52 (1984) 557–560.
[39] X.L. Zhang, W.Y. Guo, L. Zhou, et al., J. Mater. Chem. A 9 (2021) 20530–20543.
[40] N. Zhang, J. He, W. Han, et al., J. Mater. Sci. 54 (2019) 9603–9612.
[41] J. Hu, K. Chen, Z. Yao, et al., Sci. Bull. 66 (2021) 694–707.
[42] J. Li, L. Yang, H. Zhang, et al., Chem. Eng. J. 438 (2022) 135418.
[43] Y.J. Wang, Y. Pan, L. Wang, et al., Mater. Lett. 59 (2005) 3021–3026.
[44] J. Qiu, X. Liu, R. Chen, Adv. Funct. Mater. 30 (2020) 1909392.
[45] Q. Song, J. Liang, S. Liu, et al., Nano Res. 16 (2023) 403–410.
[46] K. Liu, M. Wu, H. Jiang, et al., J. Mater. Chem. A 8 (2020) 18802–18809.
[47] W. Huang, P. Wang, X. Liao, et al., Energy Storage Mater. 33 (2020) 416–422.
[48] S.T. Gunday, E. Cevik, A. Yusuf, et al., J. Energy Storage 21 (2019) 672–679.
[49] Y.J. Wang, Y. Pan, D. Kim, J. Power Sources 159 (2006) 690–701.
[50] X. Sun, W. Xu, X. Zhang, et al., J. Energy Chem. 52 (2021) 170–180.